Earth's Future

RESEARCH ARTICLE
10.1029/2020EF001898

Cold-Season Arctic Amplification Driven by Arctic Ocean-Mediated Seasonal Energy Transfer

Eui-Seok Chung[1,2,3], Kyung-Ja Ha[2,4], Axel Timmermann[2,3], Malte F. Stuecker[5], Tamas Bodai[2,3], and Sang-Ki Lee[6]

[1]Division of Atmospheric Sciences, Korea Polar Research Institute, Incheon, South Korea, [2]Center for Climate Physics, Institute for Basic Science, Busan, South Korea, [3]Pusan National University, Busan, South Korea, [4]Department of Atmospheric Sciences, Pusan National University, Busan, South Korea, [5]Department of Oceanography and International Pacific Research Center, School of Ocean and Earth Science and Technology, University of Hawai'i at Mānoa, Honolulu, HI, USA, [6]Atlantic Oceanographic and Meteorological Laboratory, NOAA, Miami, FL, USA

Abstract The Arctic warming response to greenhouse gas forcing is substantially greater than the rest of the globe. It has been suggested that this phenomenon, commonly referred to as Arctic amplification, and its peak in boreal fall and winter result primarily from the lapse-rate feedback, which is associated with the vertical structure of tropospheric warming, rather than from the sea-ice albedo feedback, which operates mainly in summer. However, future climate model projections show consistently that an overall reduction of sea-ice in the Arctic region leads to a gradual weakening of Arctic amplification, thereby implying a key role for sea-ice albedo feedback. To resolve this apparent contradiction, we conduct a comprehensive analysis using atmosphere/ocean reanalysis data sets and a variety of climate model simulations. We show that the Arctic Ocean acts as a heat capacitor, storing anomalous heat resulting from the sea-ice loss during summer, which then gets released back into the atmosphere during fall and winter. Strong air-sea heat fluxes in fall/winter in sea-ice retreat regions in conjunction with a stably stratified lower troposphere lead to a surface-intensified warming/moistening, augmenting longwave feedback processes to further enhance the warming. The cold-season surface-intensified warming/moistening is found to virtually disappear if ocean-atmosphere-sea ice interactions are suppressed, demonstrating the importance of ice insulation effect and ocean heat uptake/release. These results strongly suggest that the warm-season ocean heat recharge and cold-season heat discharge link and integrate the warm and cold season feedbacks, and thereby effectively explain the predominance of the Arctic amplification in fall and winter.

Plain Language Summary The Arctic warms faster than the rest of our planet. Interestingly, this accelerated warming is most pronounced in boreal fall and winter, when the sea-ice albedo feedback is not active due to a lack of sunshine, which has led numerous studies to emphasize the role of longwave feedback processes. Here, we present observational and modeling evidence that the seasonal evolution of Arctic amplification cannot be explained by a single mechanism such as lapse-rate feedback or sea-ice albedo feedback. We show that ocean-atmosphere heat exchanges associated with sea-ice reduction are essential for Arctic amplification and its seasonality. In particular, our analysis shows that the ocean heat capacitor mechanism links and integrates the warm and cold season feedbacks, thereby explaining the seasonal evolution of Arctic amplification, and its peak in the cold season. This connected nature of climate feedback processes in conjunction with insulation effect of sea ice implies a substantial weakening of Arctic amplification and its seasonal contrast in a future ice-free climate as well as during ice-free states in the geological past.

Key Points:

- Arctic warming amplification and its peak in fall and winter cannot be explained by a single mechanism such as lapse-rate feedback
- Positive local longwave feedback processes in fall and winter are intricately linked to ocean-to-atmosphere heat and moisture fluxes
- The cold-season peak can be explained by the ocean heat capacitor mechanism that links and integrates the warm and cold season feedbacks

Supporting Information:

- Supporting Information S1

Correspondence to:
K.-J. Ha,
kjha@pusan.ac.kr

Citation:
Chung, E.-S., Ha, K.-J., Timmermann, A., Stuecker, M. F., Bodai, T., & Lee, S.-K. (2021). Cold-season Arctic amplification driven by Arctic ocean-mediated seasonal energy transfer. *Earth's Future*, *9*, e2020EF001898. https://doi.org/10.1029/2020EF001898

Received 9 NOV 2020
Accepted 17 DEC 2020

1. Introduction

During recent decades, the Arctic has been warming at a much faster rate than the global average. This warming amplification in the Arctic is one of the most robust features of climate change projections in response to greenhouse gas (GHG) forcing (e.g., IPCC, 2013; Manabe & Wetherald, 1975). Yet, as illustrated in Figure 1a, the Arctic exhibits also the largest intermodel spread in the amplitude of the projected warming, partly due to an incomplete understanding of the physical processes governing the Arctic climate system.

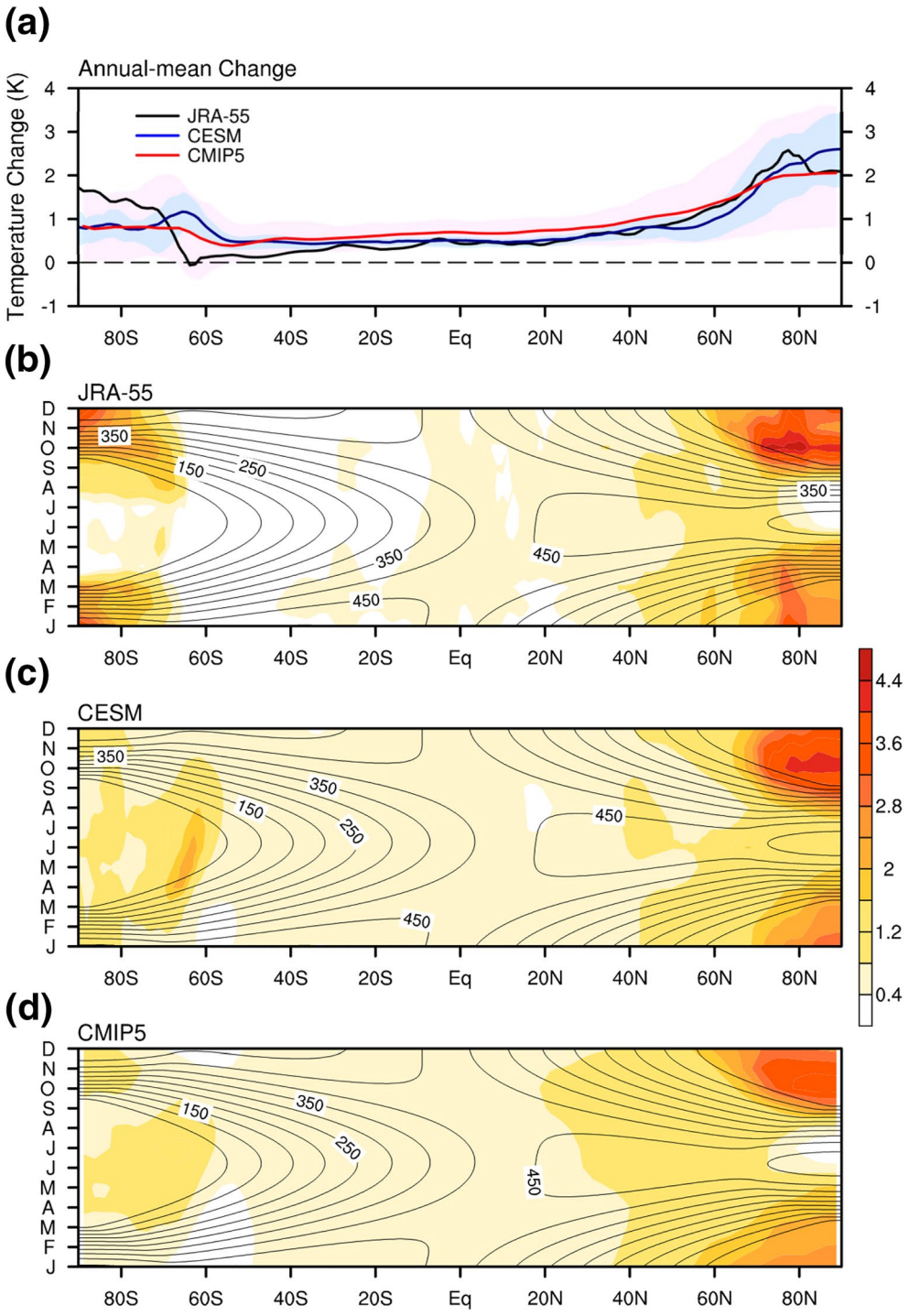

Figure 1. Arctic amplification in reanalysis and model simulations. (a) Annual-mean, zonal-mean surface air temperature change (unit: K) between 1958–1977 and 1998–2017 as a function of latitude for JRA-55 (black), CESM Large Ensemble Project (blue), and CMIP5 models (red). For model simulations, line denotes the ensemble mean or multimodel mean change under the historical and RCP8.5 scenarios, with associated shading representing a minimum-to-maximum range. (b) Distribution of the zonal-mean surface air temperature change (unit: K) as a function of season and latitude for JRA-55. (c) Same as in (b), but for the ensemble-mean change from the CESM Large Ensemble Project. (d) Same as in (b), but for the multimodel mean change of 22 CMIP5 models. Solid lines in panels (b–d) represent incoming mean solar radiation at the top of the atmosphere (TOA, unit: W m^{-2}).

There is an ongoing debate on the primary cause of Arctic amplification (e.g., Boeke & Taylor, 2018; Dai et al., 2019; Goosse et al., 2018; Graversen et al., 2008; Holland & Bitz, 2003; Laîné et al., 2016; Lu & Cai, 2010; Pithan & Mauritsen, 2014; Screen & Simmonds, 2010a; Screen et al., 2012; Stuecker et al., 2018; P. C. Taylor et al., 2013; Winton, 2006). Based on the fact that sea ice/snow-covered surfaces reflect a substantial amount of incoming solar radiation, the surface albedo feedback has been regarded as the main contributor to Arctic amplification (e.g., Hall, 2004; Holland & Bitz, 2003; Manabe & Wetherald, 1975; Screen & Simmonds, 2010b). However, in both observations and model simulations, the warming arising from GHG forcing is greatest in boreal fall (SON) and winter (DJF, hereafter referred to as cold season) during which the surface albedo feedback is nearly inactive due to the lack of incoming solar radiation (Figures 1b–1d). Moreover, previous studies showed that Arctic amplification can occur even without surface albedo feedback in idealized model simulations (e.g., Alexeev et al., 2005; Cai & Tung, 2012; Graversen & Wang, 2009; Russotto & Biasutti, 2020). These discrepancies in our basic understanding and in observations/models have led numerous studies to emphasize the role of either positive local longwave (LW) feedback processes (e.g., Bintanja et al., 2011; Graversen & Wang, 2009; Lu & Cai, 2009a; Pithan & Mauritsen, 2014; Stuecker et al., 2018; P. C. Taylor et al., 2015; Vavrus, 2004; Winton, 2006) or enhanced poleward energy transport from lower latitudes (e.g., Gong et al., 2017; Graversen et al., 2008; Khodri et al., 2001; Lee et al., 2017; Spielhagen et al., 2011). Especially, the lapse-rate feedback associated with the vertical structure of tropospheric warming has been suggested as the main contributor (Pithan & Mauritsen, 2014; Stuecker et al., 2018). However, the vertical warming structure that leads to positive lapse-rate feedback in the cold season is intricately connected to sea ice changes (e.g., Boeke et al., 2020; Feldl et al., 2020; Manabe & Stouffer, 1980): Summer sea-ice loss in response to GHG forcing leads to intensified ocean mixed layer heating, followed by an early winter increase in surface turbulent heat flux into the atmosphere. In line with this connection, a recent study (Dai et al., 2019) showed that projected Arctic warming greatly weakens when there is no sea-ice loss, arguing that Arctic amplification is closely related to ocean heat release associated with sea-ice loss (e.g., Bintanja & van der Linden, 2013; Boeke & Taylor, 2018; Deser et al., 2010; Kim et al., 2016, 2019; Screen & Simmonds, 2010a, 2010b; Serreze & Francis, 2006; Serreze et al., 2009; P. C. Taylor et al., 2018). This apparent disagreement on the physical processes leading to Arctic amplification undermines our confidence in model-projected future climate change in that Arctic climate change could exert a substantial impact on global climate.

We emphasize that these processes invoked to explain Arctic amplification might not be independent of each other (e.g., Boeke et al., 2020; Feldl et al., 2017, 2020; Graversen et al., 2014). By analyzing idealized model simulations, Graversen et al. (2014) and Feldl et al. (2017) have shown that in terms of the annual mean and zonal mean, the lapse-rate feedback is intricately connected to surface albedo feedback in the polar regions. Conversely, increased downward LW radiation due to LW feedbacks or enhanced poleward energy transport from lower latitudes can lead to a cold-season melting or delayed growth of sea ice through surface warming, which is expected to induce enhanced heat release from the open ocean given the insulation effect of sea ice (e.g., Deser et al., 2010). Therefore, an important question to address is whether sea-ice reduction and resulting anomalous seasonal ocean heat uptake/release in sea-ice retreat regions are indeed essential for Arctic amplification and its seasonality. A related question is whether the cold-season maximum of Arctic amplification can be accounted for by the LW feedbacks (and/or enhanced poleward energy transport from lower latitudes) alone without heat and moisture release from sea-ice retreat regions. Addressing these questions would help to resolve the ongoing debate on the primary cause of Arctic amplification and its peak in the cold season.

2. Materials and Methods

2.1. Data and Model Simulations

As a proxy for observations, we used multiple reanalysis/reconstructed data sets, the Japanese 55-year Reanalysis (JRA-55, Kobayashi et al., 2015), the European Centre for Medium-Range Weather Forecasts' Ocean Reanalysis System 5 (ORA-S5, Zuo et al., 2019), and the Hadley Centre Sea Ice and Sea Surface Temperature (HadISST, Rayner et al., 2003). To determine the primary causes of Arctic amplification and its seasonality, the observation and reanalysis-based changes are compared with model-simulated changes from the Community Earth System Model (CESM) Large Ensemble Project (Kay et al., 2015), in which the CESM1

model with CAM5.2 as its atmospheric component is integrated with slightly different initial conditions in the atmospheric state under the historical (up to 2005) and RCP8.5 (2006–2100) emission scenarios of the Coupled Model Intercomparison Project phase 5 (CMIP5). Model simulation output for 39 ensemble members is used in this study. Simulated changes from climate models participating in CMIP5 (K. E. Taylor et al., 2012) are also analyzed to assess the robustness of the CESM-based results. The CMIP5 models analyzed in this study are listed in Table S1.

Atmosphere-only model simulations from the Facility for Weather and Climate Assessments (FACTS, Murray et al., 2020) are used to explore whether ocean heat uptake/release in sea-ice retreat regions is a prerequisite for amplified cold-season Arctic warming. Two experiments with CAM5.1 using the Atmospheric Model Intercomparison Project (AMIP, Gates et al., 1999) boundary conditions are analyzed along with relevant coupled model simulation (i.e., CESM Large Ensemble Project). In the control AMIP experiment, CAM5.1 is integrated with observed time-varying SSTs, sea ice concentrations, and external forcing agents (RCP6 forcing scenario after 2005) prescribed. The second experiment, referred to as the Clim_Polar AMIP experiment in this study, is the same as the control experiment, but with climatological sea ice and polar SSTs prescribed. More specifically, sea ice concentration is set to a repeating seasonal cycle of 1979–1989 in this counterfactual experiment. In the case of polar SSTs, SST is prescribed in three ways depending on the 1979–1989 climatological sea-ice coverage: SST is set to (1) −1.8°C for grid points where the mean sea-ice fraction of a given month is 1, (2) the value of 1979–1989 SST climatology of a given month for grid points where the mean sea-ice fraction for that month is greater than 0 but less than 1, and (3) observed time-varying monthly value for the grid points where the 1979–1989 mean sea-ice fraction is 0 (e.g., the Norwegian Sea). Hence, any difference in the simulated Arctic climate between the two AMIP experiments can be attributed primarily to observed changes in sea ice and SST in the Arctic. Each experiment consists of 20 ensemble members. Table S1 summarizes the model experiments analyzed in this study.

2.2. Energy Budget Decomposition

Change in the net downward radiative flux at the top of the atmosphere (TOA) averaged over the Arctic between two time periods (ΔN) can be decomposed into imposed radiative forcing (RF) and radiative flux change (ΔR) arising from changes in feedback variables such as temperature (T), water vapor (WV), surface albedo (α), and clouds (C), i.e.,

$$\Delta N = RF + \Delta R_T + \Delta R_{WV} + \Delta R_\alpha + \Delta R_C. \quad (1)$$

The ΔR_T term, which represents the impact of surface and tropospheric temperature changes on TOA LW radiative flux, can be decomposed into two terms, the Planck response term (ΔR_{PL}) due to vertically uniform temperature change, which is set to be the surface air temperature change, and the lapse-rate feedback term (ΔR_{LR}) due to vertically nonuniform temperature change (e.g., Pithan & Mauritsen, 2014; Shell et al., 2008; Soden & Held, 2006; Soden et al., 2008; Stuecker et al., 2018).

Assuming that the heat storage is much smaller for land, snow, and sea ice compared to the ocean, change in the ocean heat storage and transport (ΔH) can be approximately written as

$$\Delta H = \Delta SW_d + \Delta SW_u + \Delta LW_d + \Delta LW_u + \Delta SH + \Delta LH, \quad (2)$$

where SW, LW, SH, and LH are surface shortwave and LW radiative flux, surface sensible and latent heat flux, respectively, and the subscript d and u denote downward and upward, respectively. The sign convention in Equations 1 and 2 is such that downward fluxes are positive. Although we do not separate the ocean heat storage component from the oceanic transport component, previous studies showed or assumed that model-projected heat transport change in response to GHG forcing is smaller than heat storage change in the upper Arctic Ocean (e.g., Bintanja & van der Linden, 2013; Boeke & Taylor, 2018; Laîné et al., 2016). However, it does not mean that the ocean heat transport plays a minor role in Arctic amplification. A recent study (Beer et al., 2020), for instance, proposed that enhanced vertical heat flux across the halocline in regions with sea ice can lead to increased ocean heat transport into the Arctic, which in turn contributes to Arctic amplification.

Assuming that the storage of heat in the atmosphere is negligible on time scales under consideration, the change in atmospheric energy convergence within the Arctic region due to atmospheric heat transport (ΔAEC) can be related to Arctic-mean changes in ocean heat storage and transport and TOA net downward radiative flux, as follows:

$$\Delta \mathrm{AEC} = \Delta \mathrm{H} - \Delta \mathrm{N}. \tag{3}$$

Eliminating ΔN by using Equations 1 and 3 leads to the following equation:

$$\mathrm{RF} + \Delta \mathrm{R}_{\mathrm{PL}} + \Delta \mathrm{R}_{\mathrm{LR}} + \Delta \mathrm{R}_{\mathrm{WV}} + \Delta \mathrm{R}_{\alpha} + \Delta \mathrm{R}_{\mathrm{C}} - \Delta \mathrm{H} + \Delta \mathrm{AEC} = 0. \tag{4}$$

Using the radiative kernel method (Shell et al., 2008; Soden & Held, 2006; Soden et al., 2008), in which a radiative kernel represents the change in TOA radiative flux caused by a small perturbation of a given climate variable x (i.e., $\partial \mathrm{R}/\partial x$), the Planck response term ($\Delta \mathrm{R}_{\mathrm{PL}}$) can be represented as the product of surface air temperature change and the temperature kernel (i.e., $\partial \mathrm{R}/\partial \mathrm{T}$). Hence, as derived in previous studies (e.g., Lu & Cai, 2009a; Pithan & Mauritsen, 2014; Stuecker et al., 2018), the Arctic-mean surface air temperature change can be approximated as follows:

$$\Delta \mathrm{TAS} = -\lambda_{\mathrm{PL}}{}^{-1} \cdot \left(\mathrm{RF} + \Delta \mathrm{R}_{\mathrm{LR}} + \Delta \mathrm{R}_{\mathrm{WV}} + \Delta \mathrm{R}_{\alpha} + \Delta \mathrm{R}_{\mathrm{C}} - \Delta \mathrm{H} + \Delta \mathrm{AEC}\right) + \varepsilon, \tag{5}$$

where the constant λ_{PL} is defined as $\partial \mathrm{R}/\partial \mathrm{T}$ over the Arctic and ε denotes a residual term. Equation 5 indicates that in addition to imposed RF, increases in TOA downward radiative flux induced by feedback processes (LR, WV, α, and C), northward energy transport (AEC) or ocean-to-atmosphere heat release (H) lead to warming in Arctic surface air temperature.

Given that the surface upward LW radiative flux with surface temperature $\mathrm{T_s}$ is $\varepsilon\sigma T_{\mathrm{s}}^4$ (ε denotes the surface emissivity and σ is the Stefan-Boltzmann constant), the following equation can be derived from Equation 2 by replacing the $\Delta \mathrm{LW_u}$ term by $-4\varepsilon\sigma T_{\mathrm{s}}^3 \Delta T_{\mathrm{s}}$ (e.g., Boeke & Taylor, 2018; Lee et al., 2017; Lu & Cai, 2009b):

$$\Delta T_{\mathrm{s}} = \frac{1}{4\varepsilon\sigma T_{\mathrm{s}}^3} \cdot \left(\Delta \mathrm{SW_d} + \Delta \mathrm{SW_u} + \Delta \mathrm{LW_d} - \Delta \mathrm{H} + \Delta \mathrm{SH} + \Delta \mathrm{LH}\right) \tag{6}$$

where the $\Delta \mathrm{LW_d}$ term on the right-hand side is the sum of the LW feedbacks (i.e., temperature, water vapor, and cloud) and imposed RF from a surface perspective. It is noted that $\Delta \mathrm{T_s}$ may not be identical to ΔTAS. This is because increased ocean-to-atmosphere turbulent heat fluxes warm the atmosphere at the expense of the surface, and vice versa.

3. Results

3.1. Seasonal Variation of Warming and Moistening in the Arctic

Changes in surface air temperature between 1958–1977 and 1998–2017 are computed from JRA-55, the CESM Large Ensemble Project, and 22 climate models participating in CMIP5. Interensemble spread and intermodel spread are substantial in the Arctic (Figure 1a and Figure S1), but model-simulated Arctic amplification is largely consistent with the reanalysis data set (Figure 1) and the role of external forcings (mainly GHG forcing) in recent observed Arctic climate change (Figure S2). Additional analysis using a preindustrial control simulation output suggests that noticeable warming and cooling episodes can occur in the Arctic as a result of internal variability (Figure S1). However, the reanalysis-based and model-simulated Arctic warming over the analysis period and its seasonality (Figures 1b–1d) cannot be explained by internal variability alone (Figure S1).

The spatial distribution of the surface air temperature changes from JRA-55 for August, October, and December (Figures 2a–2c) indicates that air temperature over the Arctic Ocean exhibits enhanced warming in October with marked spatial inhomogeneity. However, the warming is almost muted in August during which we expect the largest immediate effect of the sea-ice albedo feedback because incoming mean solar radiation and sea-ice responses are the strongest. Note that the seasonal warming differences are not well pronounced over the land regions. These characteristics indicate that an annual-mean, Arctic-mean

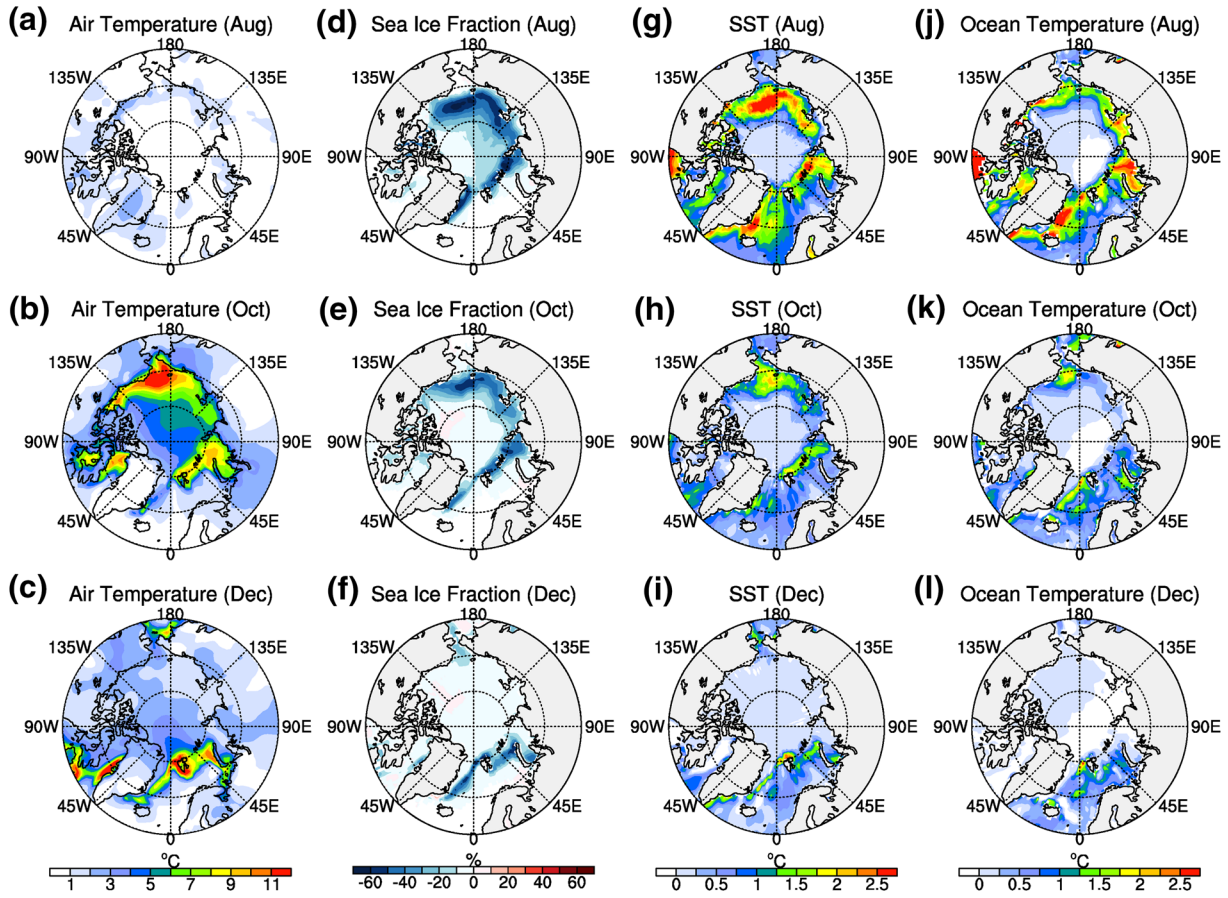

Figure 2. Spatial patterns of temperature and sea ice changes in reanalysis/reconstructed data sets. (a–c) Surface air temperature change (unit: °C, JRA-55) between 1958–1977 and 1998–2017 for (a) August, (b) October, and (c) December. (d–f) Same as in (a–c), but for sea ice fraction change (unit: %, ORA-S5). (g–i) Same as in (a–c), but for sea surface temperature change (unit: °C, HadISST). (j–l) Same as in (a–c), but for ocean potential temperature change (unit: °C, ORA-S5) at a depth of ~5 m.

perspective provides only limited insights into the physical mechanisms responsible for the strongly seasonally modulated Arctic amplification.

The spatial pattern of surface air temperature change is compared to that for sea-ice coverage change from ORA-S5 (Figures 2d–2f). Whereas sea-ice retreat regions do not show amplified warming in August, the amplified warming occurs most distinctly in sea-ice retreat regions in October and December. In contrast, the corresponding changes in SST (Figures 2g–2i) and ocean potential temperature at a depth of ~5 m (Figures 2j–2l) indicate that the largest ocean warming occurs in August, especially, in sea-ice retreat regions. In terms of seasonal evolution and phase relationships, the CESM ensemble-mean changes presented in Figure S3 are remarkably similar to the observation and reanalysis data sets.

To better understand the physical processes associated with the enhanced cold-season warming of the surface air, we examine the vertical profile of domain-averaged (70°N-90°N) atmospheric temperature and moisture changes. The cold-season atmospheric temperature change from JRA-55 is characterized by a surface-intensified warming structure, which is in stark contrast to warming maxima in the free troposphere in the summer season (Figure 3a). Previous studies have linked the surface-intensified warming structure to restricted mixing due to a stably stratified Arctic lower troposphere (e.g., Bintanja et al., 2011), whereas the warming maxima in the free troposphere have been attributed to enhanced poleward energy transport from lower latitudes (e.g., Chung & Räisänen, 2011; Graversen et al., 2008; Screen et al., 2012). The corresponding fractional change in specific humidity also exhibits a similar seasonal contrast in the vertical structure (Figure 3d). More specifically, whereas the cold season is characterized by enhanced moistening near the surface, the largest fractional increase is observed in the upper troposphere in the summer season.

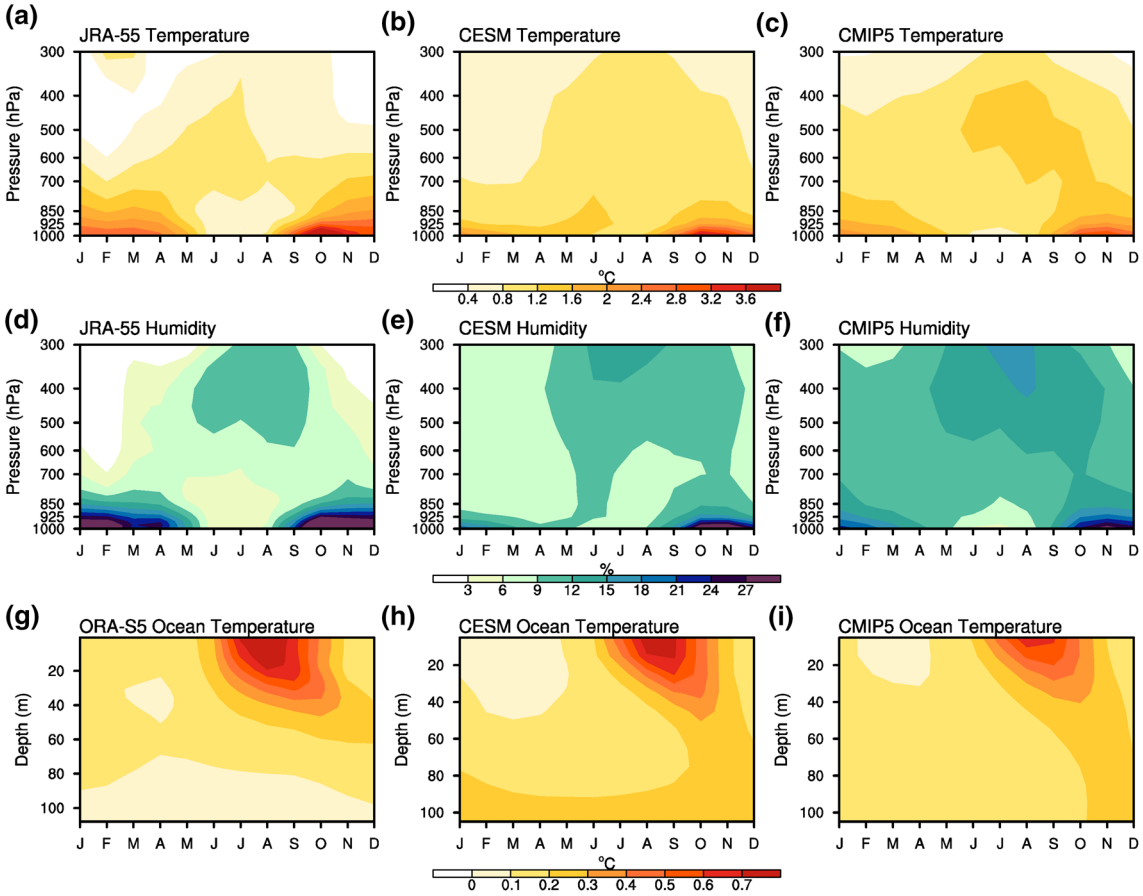

Figure 3. Temperature and humidity changes in the Arctic in response to greenhouse gas (GHG) forcing. (a–c) Arctic-mean (70°N-90°N) air temperature change (unit: °C) between 1958–1977 and 1998–2017 as a function of season and pressure for (a) JRA-55, (b) CESM Large Ensemble Project, and (c) CMIP5 models. (d–f) Same as in (a–c), but for fractional change in Arctic-mean specific humidity. (g–i) Arctic-mean ocean potential temperature change (unit: °C) as a function of season and depth for (g) ORA-S5, (h) CESM Large Ensemble Project, and (i) CMIP5 models. Note that the center and right columns denote the ensemble-mean and multimodel mean changes, respectively.

The ORA-S5 upper ocean (~50 m) potential temperature change averaged over the Arctic Ocean indicates that the largest increase in subsurface water temperatures occurs in late summer (Figure 3g), preceding the warming and moistening peak in the lowermost part of the Arctic atmosphere in fall to winter. This phase relationship appears to imply that the surface intensified warming/moistening structure is linked to anomalous ocean heat uptake and release (Manabe & Stouffer, 1980) in conjunction with the insulation effect of sea ice (e.g., Deser et al., 2010). Weaker but noticeable warming is also found in the deeper ocean, which appears to arise partly from increased solar heating of surface waters due to reduced sea ice coverage (Timmermans et al., 2018).

The corresponding ensemble-mean changes from the CESM Large Ensemble Project (Figures 3b, 3e, and 3h) and multimodel mean changes from CMIP5 models (Figures 3c, 3f, and 3i) show broadly similar seasonal variations as found in the reanalysis data sets. This consistency seems to indicate that ocean-atmosphere heat exchange processes are depicted in a similar way between JRA-55 and climate models.

3.2. Primary Factors Governing the Seasonal Evolution of Arctic Warming

An energy budget decomposition method (refer to Materials and Methods) is used to identify the main contributors to the enhanced cold-season warming. Figure 4a presents the seasonal evolution of reanalysis-based and model-simulated domain-averaged (70°N-90°N) surface air temperature change (solid lines)

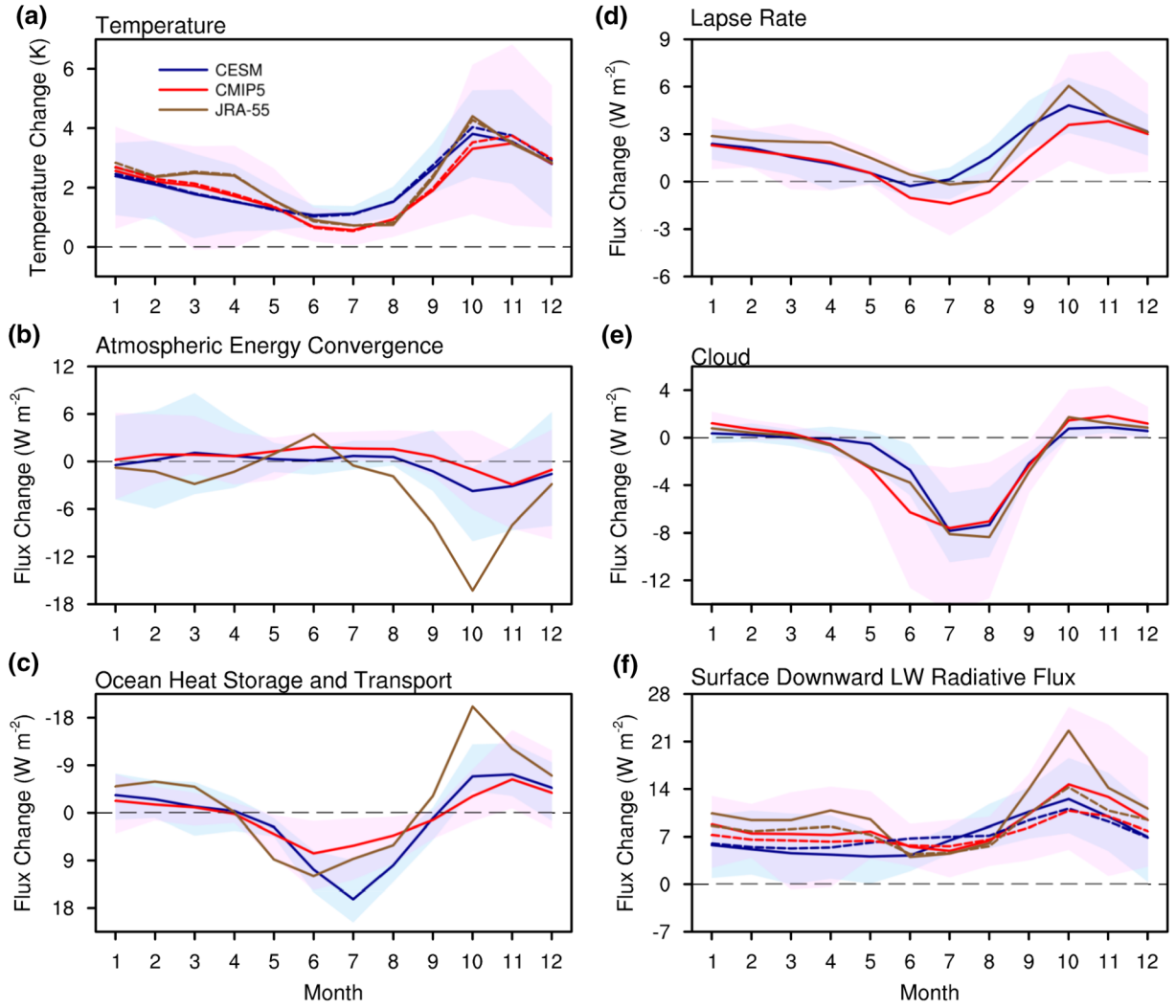

Figure 4. Phase relations between surface warming and flux changes in the Arctic. Seasonal evolution of Arctic-mean (70°N-90°N) changes between 1958–1977 and 1998–2017: (a) Surface air temperature (solid lines) and surface temperature (dashed line, unit: K), (b) Atmospheric energy convergence (unit: W m^{-2}), (c) Ocean heat storage and transport (unit: W m^{-2}), (d) Top-of-atmosphere longwave (LW) radiative flux (unit: W m^{-2}) due to lapse-rate change, (e) Cloud radiative effect (unit: W m^{-2}) at the TOA, and (f) Downward LW radiative flux at the surface for total-sky (solid lines) and clear-sky (dashed lines) conditions. Lines in blue and associated shading denote, respectively, the ensemble mean and minimum-to-maximum range of the CESM Large Ensemble Project. Lines in red and associated shading denote, respectively, the multimodel mean and intermodel range (minimum to maximum) of 22 CMIP5 models. Flux changes are defined as positive in the downward direction.

between 1958–1977 and 1998–2017, with shading denoting a minimum-to-maximum range of simulated change. In agreement with JRA-55 (solid line in brown), both the CESM ensemble mean (solid line in blue) and CMIP5 multimodel mean (solid line in red) exhibit the largest warming in fall and not in summer. Corresponding changes in surface temperature (dashed lines) exhibit a nearly identical seasonal evolution. Figure 4b shows that changes in the atmospheric energy convergence over the Arctic (ΔAEC) are positive for a subset of ensemble members and climate models, but the model-simulated forced changes imply decreased northward energy transport in the cold season. Even though there is a noticeable discrepancy in magnitude, JRA-55 also indicates reduced poleward energy transport in the cold season. Therefore, although poleward moisture transport is projected to increase in response to GHG forcing (e.g., Bintanja & Selten, 2014), it is questionable whether externally forced warming enhancement in the cold season can be attributed mainly to anomalous poleward atmospheric energy transport, partly because atmospheric dry static energy transport to the Arctic is projected to decrease and thereby compensate moisture transport changes (e.g., Hwang et al., 2011).

In contrast, both JRA-55 and climate model simulations exhibit a seasonal evolution of ocean heat storage/transport change, which is similar to that for temperature change (Figure 4c). A decomposition of the ocean heat storage/transport term (Figure S4), in conjunction with the phase relationships shown in Figure 3, implies that most of the summer energy surplus due to sea ice reduction is sequestered in the upper Arctic Ocean and then a large fraction of the accumulated heat is released back into the atmosphere, mainly in the form of turbulent heat fluxes (and LW radiative flux for CESM), contributing to the enhanced cold-season surface warming (e.g., Boeke & Taylor, 2018; Dai et al., 2019; Manabe & Stouffer, 1980; P. C. Taylor et al., 2018). This suggests that the apparent seasonal phase inconsistency between TOA radiative flux and temperature changes is mainly due to the seasonally paced ocean heat uptake/release process associated with sea-ice reduction.

The downward LW radiative flux changes at the TOA due to atmospheric lapse-rate changes are estimated by employing the radiative kernel method (Shell et al., 2008; Soden & Held, 2006; Soden et al., 2008). The estimated radiative flux changes are then averaged over the domain 70°N-90°N (Figure 4d). The resulting TOA radiative flux changes due to the lapse-rate feedback (ΔR_{LR}) exhibit positive values in the cold season, which is in line with a surface-intensified warming structure. On the other hand, the summer season exhibits near-zero or slightly negative values. Although opposing characteristics of the lapse-rate feedback between the Arctic (positive) and tropics (negative) have been suggested as the primary cause of annual-mean Arctic amplification (Pithan & Mauritsen, 2014; Stuecker et al., 2018), Equation 5 indicates that the cold-season ocean-to-atmosphere heat release, which is mainly in the form of surface turbulent heat fluxes (Figure S4), accounts for a large portion (~40%–90%) of the enhanced cold-season near-surface warming from a TOA perspective.

Cloud changes could also contribute to the enhanced cold-season warming by reducing outgoing LW radiative flux at the TOA. Thus, we analyzed changes in cloud radiative effect (CRE), which is defined as the difference between TOA net downward radiative flux for average atmospheric conditions and cloud-free conditions. Although a quantitative discrepancy exists between the cloud feedback and CRE change due to the masking effects of clouds on noncloud feedback terms (Kay & Gettelman, 2009; Soden et al., 2004), the CRE change has been used as a proxy for the cloud feedback (e.g., Shell et al., 2008; Soden et al., 2008). Figure 4e shows that the seasonal evolution of warming is partly related to cloud changes. However, comparisons with Figures 4c and 4d imply that cloud changes are unlikely to be the primary contributor, from a TOA perspective, to the enhanced cold-season warming, in agreement with earlier studies based on model simulations (e.g., Middlemas et al., 2020; Pithan & Mauritsen, 2014; Stuecker et al., 2018). From a TOA perspective, the contribution of water vapor feedback to enhanced cold-season warming is also markedly smaller than the ocean heat storage and transport term (not shown), because the enhanced moistening is confined in the lower troposphere (e.g., Figure 3e).

In the Arctic, radiative flux changes at the TOA may not be directly translated into surface temperature change (e.g., Boeke & Taylor, 2018; Pithan & Mauritsen, 2014). Therefore, we also examine the seasonal evolution of surface warming from a surface energy budget perspective. According to Equation 6, the enhanced cold-season surface warming can be induced by increased ocean heat discharge as well as increased downward LW flux at the surface. However, as shown in Figure S4, increased ocean heat discharge is accompanied by increased ocean-to-atmosphere turbulent heat fluxes that act to cool the surface. Therefore, as noted in previous studies (e.g., Boeke & Taylor, 2018; Lee et al., 2017; Lu & Cai, 2009b), increased downward LW flux at the surface is the main contributor from a surface energy budget perspective (Figure 4f). A comparison of clear-sky LW flux change (dashed lines) with total-sky case (solid lines) implies a cloud-induced enhancement of downward LW radiative flux at the surface for JRA-55 (Figure 4f).

Figure 4 indicates a consistency between JRA-55 and model simulations in the seasonal evolution of the physical processes linked to the enhanced cold-season Arctic warming. However, nonnegligible quantitative discrepancies exist in these processes in the fall season, which can arise not only from model deficiency but also from potential errors of reanalysis-based fluxes (e.g., P. C. Taylor et al., 2018). Given these uncertainties, observation-based benchmarks are needed to more adequately constrain the physical processes depicted in climate models.

In agreement with previous studies (e.g., Boeke & Taylor, 2018; Dai et al., 2019; Lee et al., 2017; Lu & Cai, 2009b; Pithan & Mauritsen, 2014; Stuecker et al., 2018), Figure 4 indicates that ocean heat storage/release

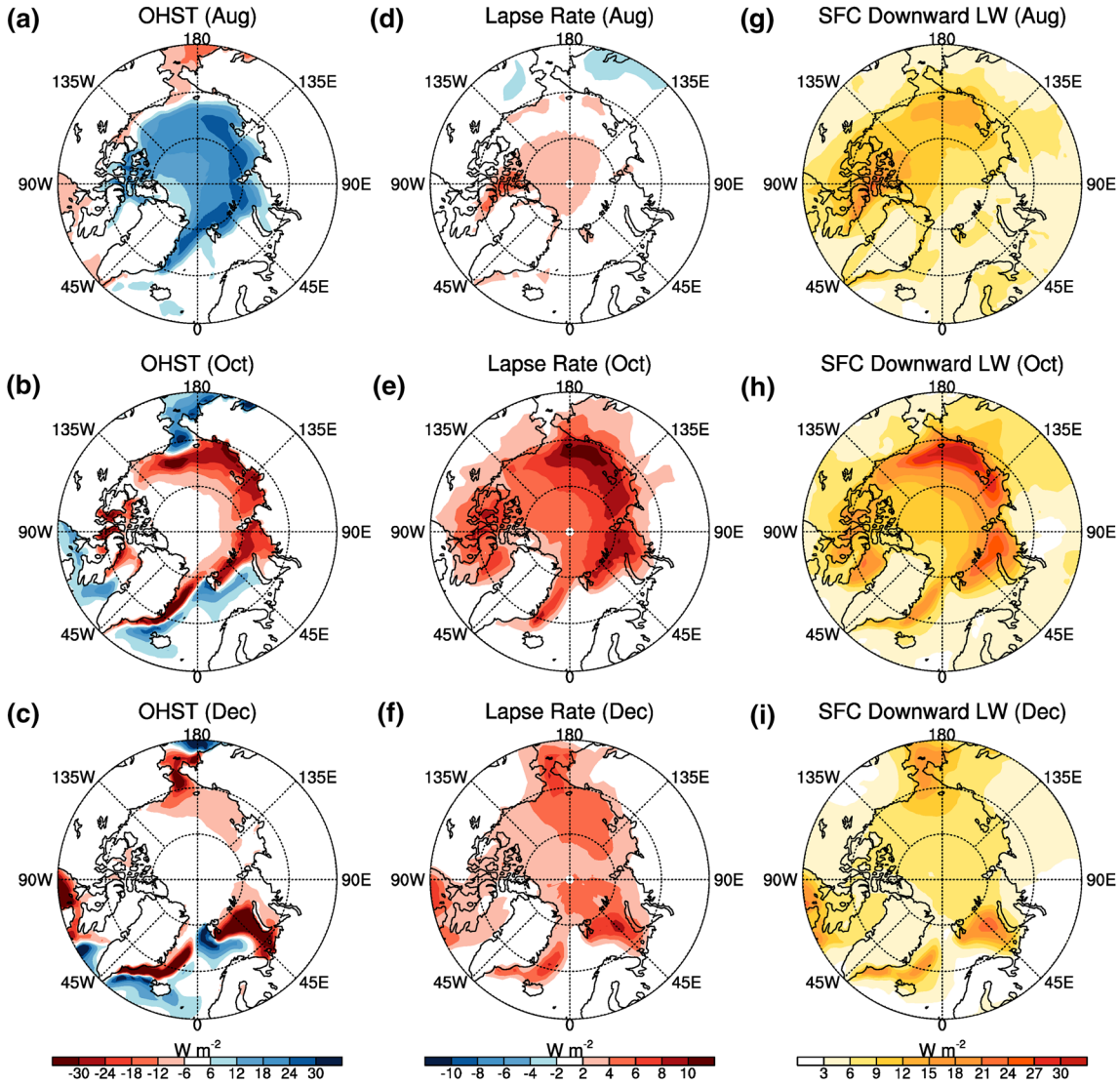

Figure 5. Relations between ocean-to-atmosphere heat release and LW feedbacks. (a–c) Spatial distribution of the ensemble-mean ocean heat storage and transport change (unit: W m^{-2}) between 1958–1977 and 1998–2017 from the CESM Large Ensemble Project for (a) August, (b) October, and (c) December. (d–f) Same as in (a–c), but for top-of-atmosphere LW radiative flux change (unit: W m^{-2}) due to lapse-rate change. (g–i) Same as in (a–c), but for change in downward LW radiative flux at the surface (unit: W m^{-2}). Flux changes are defined as positive in the downward direction.

and lapse-rate feedback (from a TOA perspective) as well as downward LW radiative flux at the surface (from a surface perspective) are the primary factors to the amplified cold-season warming. Therefore, their spatial patterns are further analyzed for the CESM ensemble mean (the CMIP5 multimodel mean changes presented in Figure S5 and the JRA-55 changes presented in Figure S6 are qualitatively consistent with the CESM ensemble mean changes). Figure 5 clearly shows that a large fraction (~65%) of the heat accumulated in the upper ocean during summer is released into the overlying atmosphere in sea-ice retreat regions during the cold season (Figures 5a–5c). For August, changes in downward LW radiative flux at the TOA due to the lapse-rate changes do not bear any spatial resemblance to the ocean heat uptake/release changes (Figure 5d). In contrast, during the cold season, distinctly positive values (but smaller in magnitude than the ocean heat storage/release term) are found over sea-ice retreat regions where ocean-to-atmosphere heat/moisture release is substantial (Figures 5e and 5f). Changes in surface downward LW radiative flux exhibit similar spatiotemporal features (Figures 5g–5i). These characteristics imply that the contribution of the lapse-rate feedback (from a TOA perspective) and surface downward LW radiative flux (from a surface perspective) to the enhanced cold-season warming is unlikely to be independent of ocean-to-atmosphere

heat and moisture fluxes (Boeke et al., 2020; Feldl et al., 2017, 2020; Graversen et al., 2014; Manabe & Stouffer, 1980). However, it is important to emphasize that they are spatially less confined and can act also in the central Arctic and not only in the sea-ice retreat regions.

3.3. Relationship Between Ocean Heat Uptake/Release and LW Feedbacks

The enhanced surface warming in fall and winter may arise mainly from LW feedbacks with ocean heat/moisture release playing a subsidiary role. In contrast, Graversen et al. (2014) showed in a climate model that locking the annual-mean surface albedo feedback leads to a weakening of the positive annual-mean lapse-rate feedback in the polar regions. In addition, Feldl et al. (2017) showed that reducing the ice albedo to eliminate the surface albedo feedback in an aquaplanet model results in a sign change of the annual-mean, zonal-mean polar lapse-rate feedback from positive to negative. These studies therefore imply the connected nature of climate feedbacks in the Arctic, at least, in terms of the annual mean. To assess the role of sea-ice reduction and ocean heat capacitor mechanism in modulating cold-season local LW feedbacks in the Arctic, model-simulated changes between 1979–1998 and 2007–2016 are compared between coupled simulations from the CESM Large Ensemble Project and two atmosphere-only runs with CAM5.1 from FACTS (Murray et al., 2020).

In terms of ensemble-mean change, both the control AMIP and coupled experiments simulate amplified warming in the Arctic (Figure 6a) with a similar seasonal evolution of Arctic-mean (70°N-90°N) surface air temperature change that peaks in October (Figure 6b). In these two experiments, the simulated warming is substantially greater over the Arctic Ocean than over the surrounding land regions (Figure 6e), with maxima located in marginal sea ice regions (Figure 6f). In contrast, the simulated Arctic warming is distinctly weaker in the Clim_Polar AMIP experiment integrated with climatological sea ice and polar SSTs, especially, in marginal sea ice regions (Figures 6a, 6b, 6e, and 6f). Given that the two AMIP experiments are identical in their representation of RF and SSTs except for sea ice and polar SSTs, these discrepancies suggest that the seasonal variation of sea-ice and SST changes is essential for the enhanced cold-season warming. Interestingly, the observed SST variability prescribed in the control AMIP experiment exhibits a similar seasonal evolution of SST change to the CESM ensemble-mean change (Figure S7).

The seasonal variation of Arctic-mean (70°N-90°N) atmospheric temperature change is also analyzed (Figure S8). Despite a substantial discrepancy in experimental design, the ensemble-mean temperature changes exhibit a similar vertical structure in summer. In particular, the warming in the free troposphere is roughly comparable in magnitude for all months, implying negligible impacts of sea ice and SST changes. However, the Clim_Polar AMIP experiment fails to capture the cold-season surface-intensified warming seen in JRA-55 and coupled model simulations (Figures 3a–3c). In addition, the cold-season lower tropospheric moistening is distinctly weaker in the Clim_Polar AMIP experiment than in the other two (Figure S9). Considering that the two AMIP experiments exhibit nearly identical vertical profiles of temperature change in the tropics and mid-latitudes (not shown) and the imposed RF is similar between the AMIP and coupled experiments, these discrepancies indicate that sea-ice reduction and the resulting anomalous seasonal ocean heat storage and release are the primary contributor to the surface-intensified vertical structure of atmospheric warming/moistening in the cold season with surface turbulent heat fluxes connecting the amplified surface warming to the lower troposphere (e.g., Bintanja & Selten, 2014; Bintanja & van der Linden, 2013; Boeke & Taylor, 2018; Dai et al., 2019; Kim et al., 2019; Manabe & Stouffer, 1980) seen in both reanalysis and coupled model simulations.

We conducted additional analysis to further understand what processes are driving these differences between the Clim_Polar AMIP and the control AMIP/coupled simulations. The ensemble-mean changes in ocean heat storage/transport and surface downward LW radiative flux for the control AMIP experiment are largely consistent with coupled model simulations in that marked increases in ocean-to-atmosphere heat release and surface downward LW radiative flux are found in sea-ice retreat regions (Figure S10). Unfortunately, due to a data availability issue, similar analysis cannot be conducted for the Clim_Polar AMIP experiment. To circumvent this challenge, changes in surface downward LW radiative flux are indirectly compared between the two AMIP simulations by examining changes in surface air temperature and fractional changes in specific humidity at 1,000 hPa. If sea-ice reduction and resulting ocean heat uptake/release play a minor role in the cold-season increase in surface downward LW radiative flux, differences between the

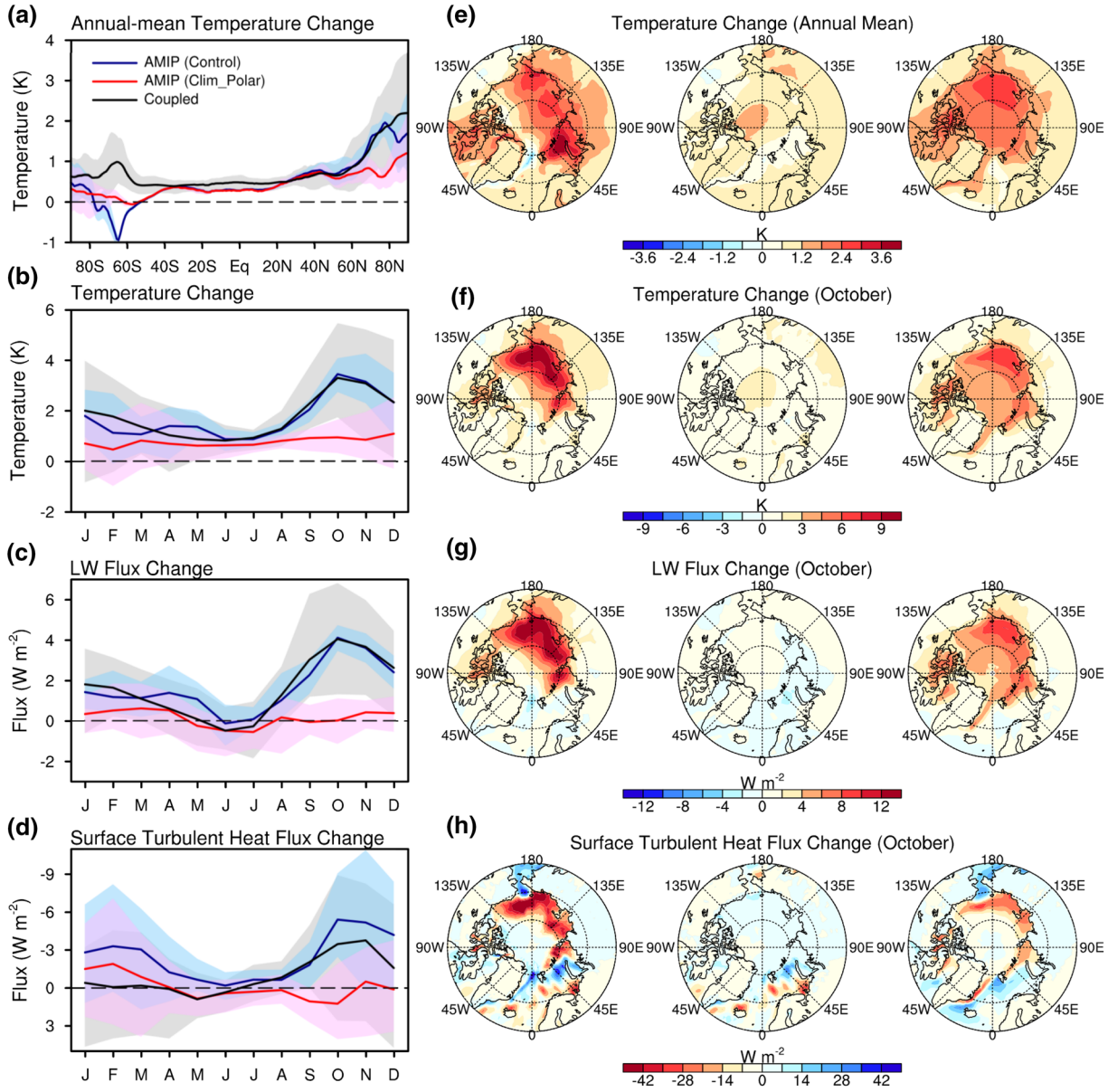

Figure 6. Contributions of Arctic sea-ice and sea surface temperature (SST) changes to amplified warming in the Arctic. (a) Latitudinal distribution of the annual-mean, zonal-mean surface air temperature change between 1979–1988 and 2007–2016 in two atmosphere-only simulations with CAM5.1 (control and Clim_Polar) and coupled model simulation (CESM Large Ensemble Project), with lines and associated shading representing the ensemble mean and minimum-to-maximum range. While CAM5.1 is integrated with observed SSTs and sea ice for the control Atmospheric Model Intercomparison Project (AMIP) simulation, climatological sea ice and polar SSTs are used to force CAM5.1 for Clim_Polar. (b) Seasonal evolution of Arctic-mean (70°N-90°N) surface air temperature change. (c) Same as in (b), but for top-of-atmosphere downward LW radiative flux change due to lapse-rate change. (d) Same as in (b), but for surface turbulent heat flux change. (e) Spatial distribution of the annual-mean surface air temperature change for (left) control AMIP, (center) Clim_Polar AMIP, and (right) coupled model simulations. (f) Same as in (e), but for surface air temperature change for October. (g) Same as in (e), but for top-of-atmosphere downward LW radiative flux change due to lapse-rate change for October. (h) Same as in (e), but for surface turbulent heat flux change for October.

two AMIP simulations are unlikely to be substantial. However, the cold-season increases in surface air temperature and humidity in sea-ice retreat regions seen in the control AMIP experiment are not captured in the Clim_Polar AMIP experiment (Figures S11 and S12), demonstrating the influence of sea-ice reduction and ocean heat uptake/release on cold-season downward LW radiative flux at the surface. Furthermore, the ensemble-mean TOA LW flux change associated with the lapse-rate change is markedly dampened in the Clim_Polar AMIP experiment (Figures 6c and 6g), supporting the argument that the lapse-rate feedback is tied to sea ice reduction and related sea-ice feedbacks (Boeke et al., 2020; Feldl et al., 2017, 2020; Graversen

et al., 2014). This dampening is especially pronounced in sea-ice retreat regions where a substantial amount of heat is released from the ocean into the atmosphere mainly in the form of surface turbulent heat fluxes in the control AMIP and coupled model simulations (Figures 6d and 6h).

It is noted that the SSTs at lower latitudes are not kept fixed in the Clim_Polar AMIP experiment, which acts to increase the meridional temperature gradient and thus poleward energy transport from lower latitudes. In addition, land surface temperatures are not constrained in both AMIP simulations, which may also affect poleward energy transport. Considering that surface turbulent heat fluxes are governed by temperature and humidity differences between the surface and atmosphere, wind speed, surface roughness, and surface radiative fluxes (e.g., P. C. Taylor et al., 2018), these confounding factors could affect the characteristics of ocean-atmosphere heat exchanges. However, the marked contrast between the Clim_Polar AMIP and the control AMIP/coupled simulations demonstrates that ocean-atmosphere heat exchanges and their modulation by sea ice regulate the cold-season LW feedbacks with surface turbulent heat flux response representing a mechanism to communicate the surface-based warming to the atmosphere.

The sea-ice insulation effect along with the close relationships between cold-season LW feedbacks and ocean heat/moisture release imply that Arctic amplification will substantially weaken in a much warmer climate because the sea-ice albedo feedback and insulation effect of sea ice (Deser et al., 2010; Screen & Simmonds, 2010a) are virtually inactive in a nearly ice-free condition. To evaluate the validity of this hypothesis, using a subset of CMIP5 models, we computed the ratio of Arctic-mean (70°N-90°N) surface air temperature change to the corresponding global-mean change with a 60-year sliding window over the period 1951–2250 (Figure S13). The time series for the multimodel mean for the annual mean (Figure S13d) and October-November-December (OND) mean (Figure S13f) show a greatly weakened Arctic amplification in the 23rd century, in which the Arctic Ocean becomes nearly ice-free in all seasons in most of the models (Figures S13a–S13c), compared to the current climate. In contrast, the ratio for June-July-August (JJA) mean rarely changes over time (Figure S13e), except for the GISS-E2-R model.

The multimodel mean temperature change normalized by the corresponding global-mean change is also computed for the period 1951–2010 and 2191–2250 (Figure 7). Compared to the period 1951–2010, the spatial maps for the period 2191–2250 clearly indicate a pronounced weakening of the warming amplification over the Arctic Ocean for the annual-mean and OND mean cases. The normalized temperature change for the latter period is still greater than 1 over the Arctic, but the magnitude of the warming amplification does not differ distinctly from that for the mid-latitude land regions. Furthermore, the pronounced seasonal contrast disappears in the latter period (Figures 7e vs. 7f in comparison to Figures 7b vs. 7c). This state dependency of Arctic amplification is also evident for the seasonal evolution of changes in surface air temperature, ocean heat storage/transport, TOA downward LW radiative flux due to the lapse-rate feedback, and surface downward LW radiative flux with the distinct cold-season peak evident in the current climate disappearing in the nearly ice-free climate (Figure S14). Although previous studies showed that enhanced northward energy transport can induce Arctic amplification even without surface albedo feedback in idealized model simulations (e.g., Alexeev et al., 2005; Cai & Tung, 2012; Graversen & Wang, 2009; Russotto & Biasutti, 2020), the marked contrast between the current climate and a much warmer climate highlights the role of the sea-ice albedo and insulation feedbacks and the ocean heat capacitor mechanism that connects the warm and cold season feedbacks.

4. Discussion and Summary

To enhance our understanding of the underlying mechanisms for Arctic amplification and its seasonality, we have analyzed the seasonal variation of Arctic warming in conjunction with that for TOA and surface energy budgets and ocean temperatures using observations/reanalysis data sets and a variety of climate model simulations. Our analysis indicates that the seasonal evolution of Arctic amplification cannot be attributed to a single mechanism (e.g., lapse-rate feedback or sea-ice albedo feedback). We suggest that the ocean heat recharge and discharge mechanism associated with sea-ice reduction links the warm and cold season feedbacks to each other, thereby explaining the seasonal evolution of amplified warming in the Arctic, and its peak in fall and winter. Figure 8 summarizes schematically the processes by which anomalous seasonal ocean heat uptake and release contributes to cold-season Arctic amplification: Initial warming in

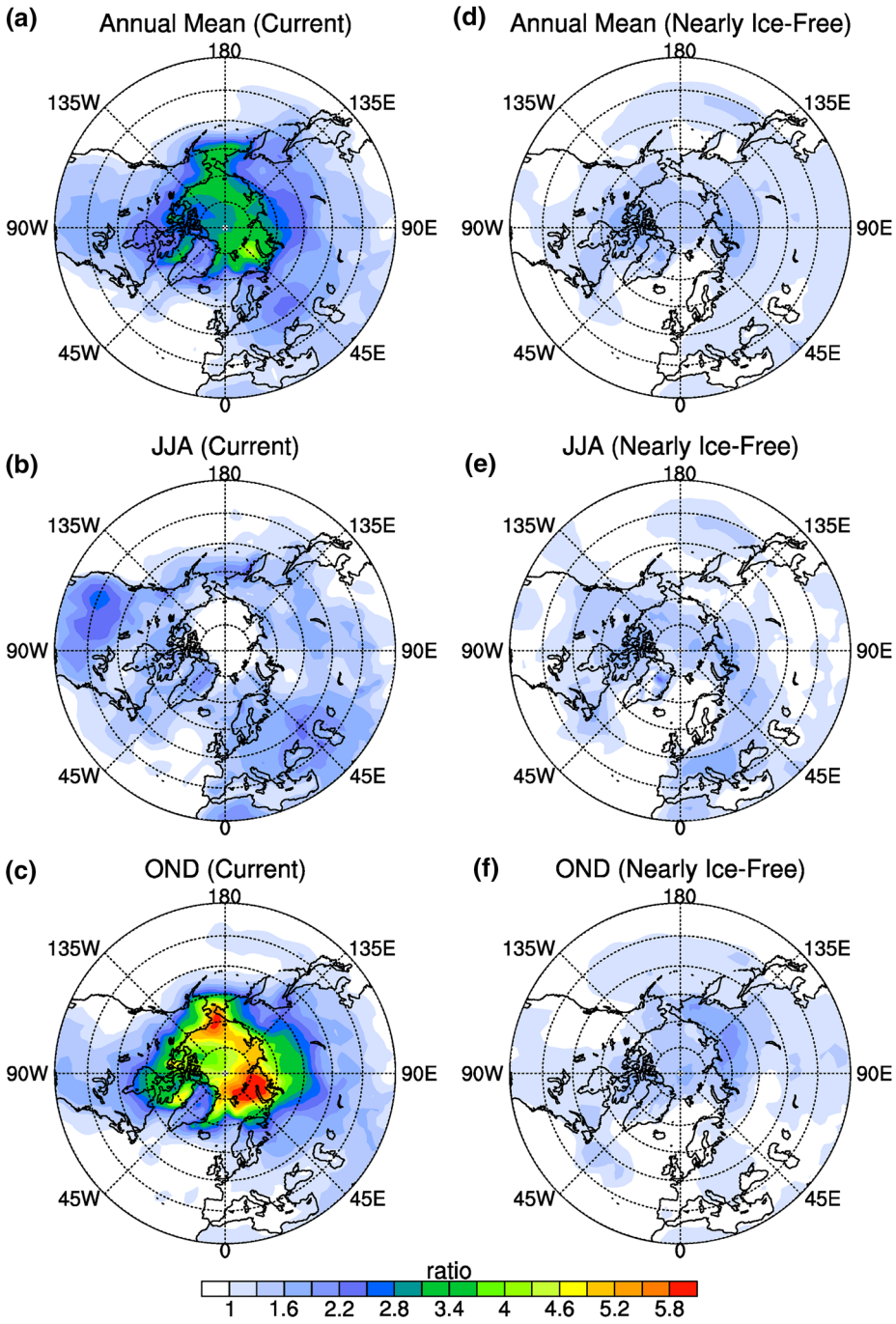

Figure 7. Dependence of Arctic amplification on base climate. (a–c) Spatial distribution of the multimodel mean of the surface air temperature change between 1951–1970 and 1991–2010 (current climate) normalized by the corresponding global-mean change for (a) Annual mean, (b) June-July-August mean, and (c) October-November-December mean. (d–f) Same as in (a–c), but for temperature change between 2191–2210 and 2231–2250 (nearly ice-free climate).

the atmosphere induced by GHG forcing leads to summer melting of sea ice and anomalous uptake of heat in the upper ocean. This process is further enhanced by the summer season positive sea-ice albedo feedback. In the subsequent months the thermal reservoir discharges, which leads to the reduction of the climatological sea-ice coverage, and intensification of the air-sea fluxes in association with the insulation effect of sea ice (e.g., Deser et al., 2010). This process is stretched out for several more months as the climatological build-

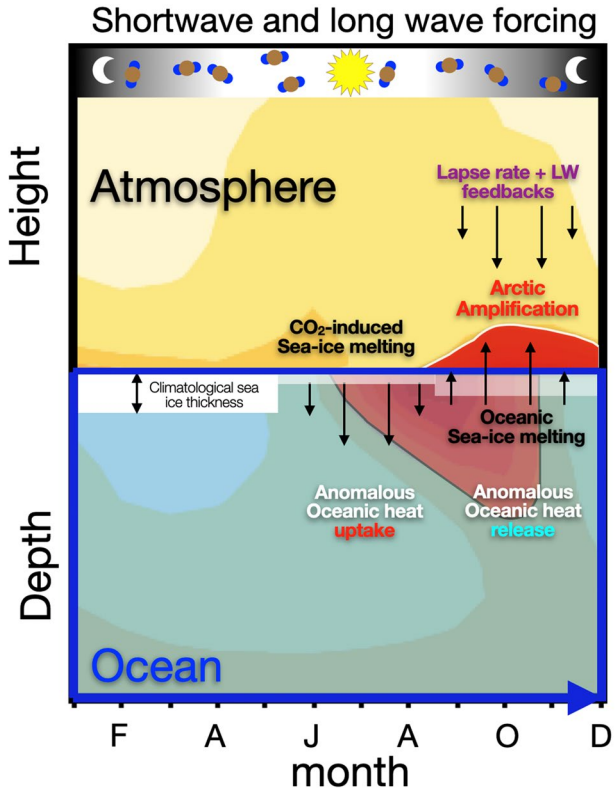

Figure 8. A schematic diagram illustrating the contribution of anomalous seasonal ocean heat uptake/release to fall/winter Arctic amplification. The upper ocean stores heat resulting from GHG-induced sea-ice loss during summer, and the accumulated heat is then released back into the atmosphere during fall and winter. Due to a stable condition in the lowermost part of the atmosphere during the cold season, a large fraction of the heat and moisture released from sea-ice retreat regions is trapped in that layer. The surface-intensified warming and moistening in turn acts to further promote LW feedback processes, including the lapse-rate feedback, to enhance the warming.

up of sea-ice insulates the upper ocean heat content (e.g., Dai et al., 2019; Deser et al., 2010). A stable condition in the cold-season Arctic lower troposphere causes a large fraction of the heat and moisture transferred from the open ocean to be trapped in the lower troposphere, which acts to augment LW feedback processes to further enhance the warming. In this regard the ocean can serve as a heat capacitor: anomalous heat pumping in summer, enabled by low seasonal sea-ice concentrations alternates with anomalous heat-discharge in fall and winter, which eventually enhances cold-season Arctic amplification (Boeke & Taylor, 2018; Dai et al., 2019; Manabe & Stouffer, 1980).

Local LW feedbacks play an important role in amplifying the cold-season warming. Yet, our analysis based on the FACTS AMIP simulations (Murray et al., 2020) indicates that local LW feedbacks are intricately linked to ocean-to-atmosphere heat and moisture fluxes, in line with previous studies (Boeke et al., 2020; Feldl et al., 2017, 2020; Graversen et al., 2014). As a result, their impacts are likely to substantially weaken if ocean-atmosphere-sea ice interactions are suppressed or muted, which seems to explain why model-projected warming substantially weakens when there is no sea-ice loss (e.g., Dai et al., 2019).

The freshening of the Arctic Ocean due to sea ice melting is likely to increase stratification, which makes the summer heat storage and subsequent heat release in fall and winter more effective. As a large amount of freshwater resulting from sea ice melting tends to accumulate within the Beaufort Gyre (e.g., Armitage et al., 2020), changes in this wind-driven ocean circulation may affect the characteristics of the ocean heat capacitor mechanism. In addition, given that observed sea-ice loss is partly due to the internal variability of the Arctic atmospheric circulation and oceanic heat transport into the Arctic Ocean (e.g., Ding et al., 2017; Zhang, 2015), the extent to which sea-ice loss and the ocean heat capacitor mechanism contribute to Arctic amplification might be affected by future changes in these factors. Nonetheless, our analysis clearly indicates that sea ice reduction and ocean heat uptake/release are essential elements for the seasonal evolution of Arctic amplification and its peak in the cold season. Given that changes in the Arctic may have far-reaching global impacts, it is of great importance to assess and improve the fidelity of these processes depicted in climate models based on accurate, long-term observations.

Data Availability Statement

JRA-55 reanalysis data can be downloaded from the JMA Data Dissemination System (https://jra.kishou.go.jp/JRA-55/index_en.html#download). ECMWF ORA-S5 data can be obtained from the University of Hamburg Integrated Climate Data Center (http://icdc.cen.uni-hamburg.de/). HadISST data can be downloaded from the Met Office Hadley Centre (https://www.metoffice.gov.uk/hadobs/hadisst/). The CESM Large Ensemble Project simulation output is available at http://www.cesm.ucar.edu/projects/community-projects/LENS/data-sets.html. The CMIP5 model output analyzed in this study can be downloaded from the Earth System Grid Federation server (https://esgf-node.llnl.gov/search/cmip5/). The FACTS CAM5.1 AMIP simulation output is available at https://www.esrl.noaa.gov/psd/repository/alias/factsdocs.

References

Alexeev, V. A., Langen, P. L., & Bates, J. R. (2005). Polar amplification of surface warming on an aquaplanet in "ghost forcing" experiments without sea ice feedbacks. *Climate Dynamics*, *24*(7-8), 655–666. https://doi.org/10.1007/s00382-005-0018-3

Armitage, T. W. K., Manucharyan, G. E., Petty, A. A., Kwok, R., & Thompson, A. F. (2020). Enhanced eddy activity in the Beaufort Gyre in response to sea ice loss. *Nature Communications*, *11*(1), 761. https://doi.org/10.1038/s41467-020-14449-z

Acknowledgments
We thank Patrick Taylor, an anonymous reviewer, and the editor for their constructive and valuable comments, which led to an improved version of the manuscript. We are grateful to the Japan Meteorological Agency, the European Centre for Medium Range Weather Forecasts, the Met Office Hadley Centre, the National Center for Atmospheric Research, and the NOAA Earth System Research Laboratory for providing their respective data sets. We acknowledge the World Climate Research Programme's Working Group on Coupled Modeling, which is responsible for the Coupled Model Intercomparison Project (CMIP), and we thank the climate modeling groups for producing and making available their model output. For CMIP, the U.S. Department of Energy's Program for Climate Model Diagnosis and Intercomparison provides coordinating support and led the development of software infrastructure in partnership with the Global Organization for Earth System Science Portals. This study was supported by the Institute for Basic Science (IBS) under IBS-RS028-D1. E.-S.C. was also supported by the project PE20090 of the Korea Polar Research Institute. This is IPRC publication 1497 and SOEST contribution 11221.

Beer, E., Eisenman, I., & Wagner, T. J. W. (2020). Polar amplification due to enhanced heat flux across the halocline. *Geophysical Research Letters*, *47*(4), e2019GL086706. https://doi.org/10.1029/2019GL086706

Bintanja, R., Graversen, R. G., & Hazeleger, W. (2011). Arctic winter warming amplified by the thermal inversion and consequent low infrared cooling to space. *Nature Geoscience*, *4*(11), 758–761. https://doi.org/10.1038/ngeo1285

Bintanja, R., & Selten, F. M. (2014). Future increases in Arctic precipitation linked to local evaporation and sea-ice retreat. *Nature*, *509*(7501), 479–482. https://doi.org/10.1038/nature13259

Bintanja, R., & van der Linden, E. C. (2013). The changing seasonal climate in the Arctic. *Scientific Reports*, *3*(1), 1556. https://doi.org/10.1038/srep01556

Boeke, R. C., & Taylor, P. C. (2018). Seasonal energy exchange in sea ice retreat regions contributes to differences in projected Arctic warming. *Nature Communications*, *9*(1), 5017. https://doi.org/10.1038/s41467-018-07061-9

Boeke, R. C., Taylor, P. C., & Sejas, S. A. (2020). On the nature of the Arctic's positive lapse rate feedback. *Geophysical Research Letters*, *48*(1), e2020GL091109. https://doi.org/10.1029/2020GL091109

Cai, M., & Tung, K.-K. (2012). Robustness of dynamical feedbacks from radiative forcing: 2% solar versus 2 × CO_2 experiments in an idealized GCM. *Journal of the Atmospheric Sciences*, *69*(7), 2256–2271. https://doi.org/10.1175/JAS-D-11-0117.1

Chung, C. E., & Räisänen, P. (2011). Origin of the Arctic warming in climate models. *Geophysical Research Letters*, *38*, L21704. https://doi.org/10.1029/2011GL049816

Dai, A., Luo, D., Song, M., & Liu, J. (2019). Arctic amplification is caused by sea-ice loss under increasing CO_2. *Nature Communications*, *10*(1), 121. https://doi.org/10.1038/s41467-018-07954-9

Deser, C., Tomas, R., Alexander, M., & Lawrence, D. (2010). The seasonal atmospheric response to projected Arctic sea ice loss in the late twenty-first century. *Journal of Climate*, *23*(2), 333–351. https://doi.org/10.1175/2009JCLI3053.1

Ding, Q., Schweiger, A., L'Heureux, M., Battisti, D. S., Po-Chedley, S., Johnson, N. C., et al. (2017). Influence of high-latitude atmospheric circulation changes on summertime Arctic sea ice. *Nature Climate Change*, *7*(4), 289–295. https://doi.org/10.1038/nclimate3241

Feldl, N., Bordoni, S., & Merlis, T. M. (2017). Coupled high-latitude climate feedbacks and their impact on atmospheric heat transport. *Journal of Climate*, *30*(1), 189–201. https://doi.org/10.1175/JCLI-D-16-0324.1

Feldl, N., Po-Chedley, S., Singh, H. K. A., Hay, S., & Kushner, P. J. (2020). Sea ice and atmospheric circulation shape the high-latitude lapse rate feedback. *npj Climate and Atmospheric Science*, *3*(1), 41. https://doi.org/10.1038/s41612-020-00146-7

Gates, W. L., Boyle, J. S., Dease, C. G., Doutriaux, C. M., Drach, R. S., Fiorino, M., et al (1999). An overview of the results of the Atmospheric Model Intercomparison Project (AMIP I). *Bulletin of the American Meteorological Society*, *80*(1), 29–56. https://doi.org/10.1175/1520-0477(1999)080<0029:AOOTRO>2.0.CO;2

Gong, T., Feldstein, S., & Lee, S. (2017). The role of downward infrared radiation in the recent Arctic winter warming trend. *Journal of Climate*, *30*(13), 4937–4949. https://doi.org/10.1175/JCLI-D-16-0180.1

Goosse, H., Kay, J. E., Armour, K. C., Bodas-Salcedo, A., Chepfer, H., Docquire, D., et al. (2018). Quantifying climate feedbacks in polar regions. *Nature Communications*, *9*(1), 1919. https://doi.org/10.1038/s41467-018-04173-0

Graversen, R. G., Langen, P. L., & Mauritsen, T. (2014). Polar amplification in CCSM4: Contributions from the lapse rate and surface albedo feedbacks. *Journal of Climate*, *27*(12), 4433–4450. https://doi.org/10.1175/JCLI-D-13-00551.1

Graversen, R. G., Mauritsen, T., Tjernström, M., Källén, E., & Svensson, G. (2008). Vertical structure of recent Arctic warming. *Nature*, *451*(7174), 53–56. https://doi.org/10.1038/nature06502

Graversen, R. G., & Wang, M. (2009). Polar amplification in a coupled climate model with locked albedo. *Climate Dynamics*, *33*(5), 629–643. https://doi.org/10.1007/s00382-009-0535-6

Hall, A. (2004). The role of surface albedo feedback in climate. *Journal of Climate*, *17*(7), 1550–1568. https://doi.org/10.1175/1520-0442(2004)017%3C1550:TROSAF%3E2.0.CO;2

Holland, M. M., & Bitz, C. M. (2003). Polar amplification of climate change in coupled models. *Climate Dynamics*, *21*(3-4), 221–232. https://doi.org/10.1007/s00382-003-0332-6

Hwang, Y.-T., Frierson, D. M. W., & Kay, J. E. (2011). Coupling between Arctic feedbacks and changes in poleward energy transport. *Geophysical Research Letters*, *38*, L17704. https://doi.org/10.1029/2011GL048546

IPCC (2013). Climate change 2013: The physical science basis. In T. F. Stocker, D. Qin, G.-K. Plattner, et al. (Eds.), *Contribution of Working Group I to the Fifth Assessment Report of the Intergovernmental Panel on Climate Change* (p. 1535). Cambridge, UK; New York, NY: Cambridge University Press.

Kay, J. E., Deser, C., Phillips, A., Mai, A., Hannay, C., Strand, G., et al. (2015). The Community Earth System Model (CESM) Large Ensemble Project: A community resource for studying climate change in the presence of internal climate variability. *Bulletin of the American Meteorological Society*, *96*(8), 1333–1349. https://doi.org/10.1175/BAMS-D-13-00255.1

Kay, J. E., & Gettelman, A. (2009). Cloud influence on and response to seasonal Arctic sea ice loss. *Journal of Geophysical Research*, *114*, D18204. https://doi.org/10.1029/2009JD011773

Khodri, M., Leclainche, Y., Ramstein, G., Braconnot, P., Marti, O., & Cortijo, E. (2001). Simulating the amplification of orbital forcing by ocean feedbacks in the last glaciation. *Nature*, *410*(6828), 570–574. https://doi.org/10.1038/35069044

Kim, K.-Y., Hamlington, B. D., Na, H., & Kim, J. (2016). Mechanism of seasonal Arctic sea ice evolution and Arctic amplification. *The Cryosphere*, *10*(5), 2191–2202. https://doi.org/10.5194/tc-10-2191-2016

Kim, K.-Y., Kim, J.-Y., Kim, J., Yeo, S., Na, H., Hamlington, B. D., & Leben, R. R. (2019). Vertical feedback mechanism of winter Arctic amplification and sea ice loss. *Scientific Reports*, *9*(1), 1184. https://doi.org/10.1038/s41598-018-38109-x

Kobayashi, S., Ota, Y., Harada, Y., Ebita, A., Moriya, M., Onoda, H., et al. (2015). The JRA-55 reanalysis: General specifications and basic characteristics. *Journal of the Meteorological Society of Japan*, *93*(1), 5–48. https://doi.org/10.2151/jmsj.2015-001

Laîné, A., Yoshimori, M., & Abe-Ouchi, A. (2016). Surface Arctic amplification factors in CMIP5 models: Land and oceanic surfaces and seasonality. *Journal of Climate*, *29*(9), 3297–3316. https://doi.org/10.1175/JCLI-D-15-0497.1

Lee, S., Gong, T., Feldstein, S. B., Screen, J. A., & Simmonds, I. (2017). Revisiting the cause of the 1989–2009 Arctic surface warming using the surface energy budget: Downward infrared radiation dominates the surface fluxes. *Geophysical Research Letters*, *44*(20), 10654–10661. https://doi.org/10.1002/2017GL075375

Lu, J., & Cai, M. (2009a). A new framework for isolating individual feedback processes in coupled general circulation climate models. Part I: Formulation. *Climate Dynamics*, *32*(6), 873–885. https://doi.org/10.1007/s00382-008-0425-3

Lu, J., & Cai, M. (2009b). Seasonality of polar surface warming amplification in climate simulations. *Geophysical Research Letters*, *36*, L16704. https://doi.org/10.1029/2009GL040133

Lu, J., & Cai, M. (2010). Quantifying contributions to polar warming amplification in an idealized coupled general circulation model. *Climate Dynamics*, *34*(5), 669–687. https://doi.org/10.1007/s00382-009-0673-x

Manabe, S., & Stouffer, R. J. (1980). Sensitivity of a global climate model to an increase of CO_2 concentration in the atmosphere. *Journal of Geophysical Research*, *85*(C10), 5529–5554. https://doi.org/10.1029/JC085iC10p05529

Manabe, S., & Wetherald, R. T. (1975). The effects of doubling the CO_2 concentration on the climate of a general circulation model. *Journal of the Atmospheric Sciences*, *32*(1), 3–15. https://doi.org/10.1175/1520-0469(1975)032%3C0003:TEODTC%3E2.0.CO;2

Middlemas, E. A., Kay, J. E., Medeiros, B. M., & Maroon, E. A. (2020). Quantifying the influence of cloud radiative feedbacks on Arctic surface warming using cloud locking in an Earth system model. *Geophysical Research Letters*, *47*(15), e2020GL089207. https://doi.org/10.1029/2020GL089207

Murray, D., Hoell, A., Hoerling, M., Perlwitz, J., Quan, X.-W., Allured, D., et al. (2020). Facility for Weather and Climate Assessments (FACTS): A community resources for assessing weather and climate variability. *Bulletin of the American Meteorological Society*, *101*(7), E1214–E1224. https://doi.org/10.1175/BAMS-D-19-0224.1

Pithan, F., & Mauritsen, T. (2014). Arctic amplification dominated by temperature feedbacks in contemporary climate models. *Nature Geoscience*, *7*(3), 181–184. https://doi.org/10.1038/ngeo2071

Rayner, N. A., Parker, D. E., Horton, E. B., Folland, C. K., Alexander, L. V., Rowell, D. P., et al. (2003). Global analyses of sea surface temperature, sea ice, and night marine air temperature since the late nineteenth century. *Journal of Geophysical Research*, *108*(D14), 4407. https://doi.org/10.1029/2002JD002670

Russotto, R. D., & Biasutti, M. (2020). Polar amplification as an inherent response of a circulating atmosphere: Results from the TRACMIP aquaplanets. *Geophysical Research Letters*, *47*(6), e2019GL086771. https://doi.org/10.1029/2019GL086771

Screen, J. A., Deser, C., & Simmonds, I. (2012). Local and remote controls on observed Arctic warming. *Geophysical Research Letters*, *39*, L10709. https://doi.org/10.1029/2012GL051598

Screen, J. A., & Simmonds, I. (2010a). Increasing fall-winter energy loss from the Arctic Ocean and its role in Arctic temperature amplification. *Geophysical Research Letters*, *37*, L16707. https://doi.org/10.1029/2010GL044136

Screen, J. A., & Simmonds, I. (2010b). The central role of diminishing sea ice in recent Arctic temperature amplification. *Nature*, *464*(7293), 1334–1337. https://doi.org/10.1038/nature09051

Serreze, M. C., Barrett, A. P., Stroeve, J. C., Kindig, D. N., & Holland, M. M. (2009). The emergence of surface-based Arctic amplification. *The Cryosphere*, *3*(1), 11–19. https://doi.org/10.5194/tc-3-11-2009

Serreze, M. C., & Francis, J. A. (2006). The Arctic amplification debate. *Climatic Change*, *76*(3-4), 241–264. https://doi.org/10.1007/s10584-005-9017-y

Shell, K. M., Kiehl, J. T., & Shields, C. A. (2008). Using the radiative kernel technique to calculate climate feedbacks in NCAR's Community Atmospheric Model. *Journal of Climate*, *21*(10), 2269–2282. https://doi.org/10.1175/2007JCLI2044.1

Soden, B. J., Broccoli, A. J., & Hemler, R. S. (2004). On the use of cloud forcing to estimate cloud feedback. *Journal of Climate*, *17*(19), 3661–3665. https://doi.org/10.1175/1520-0442(2004)017<3661:OTUOCF>2.0.CO;2

Soden, B. J., & Held, I. M. (2006). An assessment of climate feedbacks in coupled ocean-atmosphere models. *Journal of Climate*, *19*(14), 33 54–3360. https://doi.org/10.1175/JCLI3799.1

Soden, B. J., Held, I. M., Colman, R., Shell, K. M., Kiehl, J. T., & Shields, C. A. (2008). Quantifying climate feedbacks using radiative kernels. *Journal of Climate*, *21*(14), 3504–3520. https://doi.org/10.1175/2007JCLI2110.1

Spielhagen, R. F., Werner, K., Sørensen, S. A., Zamelczyk, K., Kandiano, E., Bedeus, G., et al. (2011). Enhanced modern heat transfer to the Arctic by warm Atlantic water. *Science*, *331*(6016), 450–453. https://doi.org/10.1126/science.1197397

Stuecker, M. F., Bitz, C. M., Armour, K. C., Proistosescu, C., Kang, S. M., Xie, S.-P., et al. (2018). Polar amplification dominated by local forcing and feedbacks. *Nature Climate Change*, *8*(12), 1076–1081. https://doi.org/10.1038/s41558-018-0339-y

Taylor, K. E., Stouffer, R. J., & Meehl, G. A. (2012). An overview of CMIP5 and the experiment design. *Bulletin of the American Meteorological Society*, *93*(4), 485–498. https://doi.org/10.1175/BAMS-D-11-00094.1

Taylor, P. C., Cai, M., Hu, A., Meehl, J., Washington, W., & Zhang, G. J. (2013). A decomposition of feedback contributions to polar warming amplification. *Journal of Climate*, *26*(18), 7023–7043. https://doi.org/10.1175/JCLI-D-12-00696.1

Taylor, P. C., Hegyi, B. M., Boeke, R. C., & Boisvert, L. N. (2018). On the increasing importance of air-sea exchanges in a thawing Arctic: A review. *Atmosphere*, *9*(2), 41. https://doi.org/10.3390/atmos9020041

Taylor, P. C., Kato, S., Xu, K.-M., & Cai, M. (2015). Covariance between Arctic sea ice and clouds within atmospheric state regimes at the satellite footprint level. *Journal of Geophysical Research: Atmospheres*, *120*(24), 12656–12678. https://doi.org/10.1002/2015JD023520

Timmermans, M.-L., Toole, J., & Krishfield, R. (2018). Warming of the interior Arctic Ocean linked to sea ice losses at the basin margins. *Science Advances*, *4*(8), eaat6773. https://doi.org/10.1126/sciadv.aat6773

Vavrus, S. (2004). The impact of cloud feedbacks on Arctic climate under greenhouse forcing. *Journal of Climate*, *17*(3), 603–615. https://doi.org/10.1175/1520-0442(2004)017%3C0603:TIOCFO%3E2.0.CO;2

Winton, M. (2006). Amplified Arctic climate change: What does surface albedo feedback have to do with it? *Geophysical Research Letters*, *33*, L03701. https://doi.org/10.1029/2005GL025244

Zhang, R. (2015). Mechanisms for low-frequency variability of summer Arctic sea ice extent. *Proceedings of the National Academy of Sciences of the United States of America*, *112*(15), 4570–4575. https://doi.org/10.1073/pnas.1422296112

Zuo, H., Balmaseda, M. A., Tietsche, S., Mogensen, K., & Mayer, M. (2019), The ECMWF operational ensemble reanalysis-analysis system for ocean and sea-ice: A description of the system and assessment. *Ocean Science*, *15*(3), 779–808. https://doi.org/10.5194/os-15-779-2019